RSC Advances

PAPER

View Article Online
View Journal | View Issue

Cite this: *RSC Adv.*, 2020, **10**, 30982

The noncoincidence phenomenon of acetonylacetone C=O stretching in a binary mixture and the aggregation-induced split theory†

Huigang Wang, * Hang Xu, Qiuna Liu and Xuming Zheng

This article aims to correlate the noncoincidence effect phenomenon with the aggregation state of acetylacetone C=O stretching in a binary mixture. C=O stretching noncoincidence effect (NCE) was observed not only between IR and Raman spectra but also between the isotropic and anisotropic Raman spectra of acetonylacetone. The difference in C=O stretching wavenumbers of the isotropic and anisotropic Raman spectra (NCE value) in a binary mixture at different concentrations has been calculated. We found that both isotropic and anisotropic Raman wavenumbers of C=O stretching increase with the dilution of acetonylacetone by CCl_4 while the NCE value decreases. These noncoincidence and concentration effect phenomena seem to go against the quantum theory. Herein, we proposed an aggregation-induced split (AIS) model to explain the NCE phenomenon and concentration effect. The experimental data were consistent with the DFT calculations performed at the B3LYP-D3/6-311++G (d,p) levels based on the proposed model. The dynamics of transformation from monomers to an aggregated structure can be easily controlled by tuning the concentration. Solvent dependent experiments show that the value of NCE decreased with the increase of the solvent dielectric constant at the same concentration, which is in accordance with Logan's theory.

Received 31st March 2020
Accepted 4th August 2020

DOI: 10.1039/d0ra02932g

rsc.li/rsc-advances

I. Introduction

Vibrational spectroscopy is an excellent technique for probing the nature of bonding and identifying chemical structures or phases in the analysis of chemical substances.[1–4] It has been commonly applied in industrial processes, geochemistry, and health-related chemistry fields.[5–7] Experiments have demonstrated that some polar vibrational modes present their vibration wavenumber at different positions in IR and Raman spectroscopy.[8–10] Moreover, their frequencies in isotropic and anisotropic components of Raman spectra are not in coincidence; scientists refer to these phenomena as noncoincidence effects (NCEs).[11–20] They ascribe these phenomena to transition dipole-transition dipole (TD–TD) interactions.[11–20]

Our group concentrated on these phenomena for several years. First, we discovered NCEs in C=S vibrational modes.[21,22] The difference between the isotropic and anisotropic peak frequencies of C=S stretching for ethylene trithiocarbonate was determined to be 4.60 cm^{-1}.[21] This difference decreased upon dilution. These NCEs and concentration effects made us believe that C=S stretching is not a single vibrational mode, but a complex vibrational mode that is beyond spectroscopic resolution.[22]

Matrix isolation is a powerful technique for the enhancement of spectroscopic resolution because the translational and rotational motions can freeze below 6 K.[23,24] We applied this technique to study the C=O stretching NCE behavior of acetone, the most investigated model molecule for NCE phenomena.[25,26] Acetone was isolated in an argon matrix and the Raman spectra were collected at different annealing temperatures. Single, double, and triple peaks were detected separately at different temperatures for the C=O vibration, and the isotropic and anisotropic spectra for each wavenumber overlapped fairly well with no NCE.[26] Thus, an aggregation-induced split (AIS) model has been proposed to explain the acetone C=O vibration NCE phenomenon and its concentration effect.[25,26] The polar bond vibration coupling tends to align the molecules to reduce the potential energy and increase the attraction. The alignment and reorganization stabilized the aggregation structure to form dimers, trimers or clusters. Polar bonds such as C=O, C=S, S=O, C–N, and C–O especially play an important role in these interactions. The vibration coupling between adjacent polar bonds split the degenerate vibrations to two vibrational modes: in phase vibration and out of phase

Department of Chemistry, Key Laboratory of Advanced Textiles Materials and Manufacture Technology of the Ministry of Education, Engineering Research Center for Eco-Dyeing and Finishing of Textiles of the Ministry of Education, Zhejiang Sci-Tech University, Hangzhou 310018, P. R. China. E-mail: zdwhg@163.com; hugwang@ucdavis.edu; Tel: +86-571-8684-3627

† Electronic supplementary information (ESI) available: Additional FT-Raman spectra for acetonylacetone, DFT/PCM calculation of C=O vibrational frequencies, depolarization ratios, dielectric constant (ε), dipole moments (μ)/*D*, and $\Delta\nu_{NCE}$ for acetonylacetone. See DOI: 10.1039/d0ra02932g

vibration. The pairs with prominent vibrational wavenumber difference and depolarization ratio difference produced "NCE effects" with the limited spectroscopic resolution; however, in high-resolution spectroscopy, they were well separated.[25,26] Acetylacetone is the simplest β-diketone that bears two tautomeric forms (keto and enol). Due to the existence of intramolecular hydrogen bonds,[27,28] the enol form is more stable in the gas phase or in weak polar solvents, while the keto form is more stable in polar solvents, especially protic solvents. The keto structure will form intermolecular hydrogen bonds with protic solvents. Acetylacetone is a good molecule for studying solvent effects. This article aims to investigate the solvent polarity influence on its aggregation state.

The AIS model can explain most of the NCE phenomena.[25,26,29–31] In this work, 2,5-hexanedione was chosen to investigate the C=O coupling behavior and the NCE phenomenon. 2,5-Hexanedione contains two carbonyl groups, and there are two possible C=O interactions,.intramolecular and intermolecular. Intramolecular C=O interactions have no relation to their neighboring molecules, and do not show concentration effects, while intermolecular C=O interactions show both NCE phenomena and concentration effects. In this work, the isotropic and anisotropic Raman bands of 2,5-hexanedione has been recorded and their concentration dependent behavior has been investigated to know the exact molecular interaction structure.

II. Methods

A. Materials

Acetonylacetone ($CH_3COCH_2CH_2COCH_3$, TCL, >99.0%); chloroform (AR, *shanghai San Ying* chemical reagent company).

B. Experimental setup

The experimental setup for Raman spectroscopy has been used with minor modifications.[21] The experimental apparatus consists of a triple monochromator (TriVista TR557, Princeton Instruments) equipped with an argon ion laser (Coherent, CVI MELLES GRIOT) as a source of exciting light at 488 nm (75 mW output) and with a liquid nitrogen cooled CCD array (manufacturer, Princeton Instruments Inc.) allowing the wavenumber coverage of 1089 cm^{-1} and a spectral resolution (the instrumental apparatus function, FWHM) of 2.0 cm^{-1}. The accuracy in the measurement (the physical matrix pixel of the CCD camera) of band positions was 0.45 cm^{-1}. A polarization scrambler was placed between the polarizer and the spectrometer entrance slit. All measurements were carried out at room temperature (293 K) and atmospheric pressure.

The Fourier transform (FT)-Raman and FT-IR spectra were obtained with 2 cm^{-1} resolution using a FT-Raman spectrometer at 1064 nm excitation (Thermo Nicolet 960, Thermo Fisher Nicolet, USA) and a FT-IR spectrometer (Thermo Nicolet avatar 370, Thermo Fisher Nicolet, USA).

C. Computational methods

Computational chemists often pay attention to specific technologies associated with computer memory, data, storage, processor speed, and program development software, which help to understand the photophysical and photochemical characteristics of molecules. Herein, density functional (DFT) calculations and the polarizable continuum model (PCM) were used to study the vibration wavenumber of acetonyl acetone in CCl_4 and its linear dimer at B3LYP levels of theory with the 6-311++G(d,p) basis set using the Gaussian 09 program.[32] The influence of the solvent was included using the PCM and optimized geometry and the corresponding vibrational frequencies were obtained to verify the reasonable dimer structure.

We converted Raman intensity from scattering activities using the Multiwfn software (http://multiwfn.codeplex.com/releases). Multiwfn is an extremely powerful wavefunction analysis program and supports almost all of the most important wavefunction analysis methods.[33] In our case, the excitation wavenumber is 20491.80 cm^{-1} (corresponding to 488 nm) and the conversion relationship is shown as[34]

$$I_i = \frac{C(\nu_0 - \nu_i)^4 S_i}{\nu_i\left[1 - \exp\left(-\frac{hc\nu_i}{kT}\right)\right]}$$

where S_i is the Raman activity, I_i the Raman intensity, ν_o the exciting frequency in reciprocal centimeters, ν_i the vibrational frequency of the ith normal mode, h, c, and k are universal constants, and C a suitably chosen common normalization factor for all peak intensities.

With the parallel and perpendicular polarized Raman spectra we get the isotropic and anisotropic components of Raman spectra using the equation:[27]

$$I_{iso}(\nu_{VV}) = I_{VV}(\nu_{VV}) - \frac{4}{3}I_{VH}(\nu_{VH})$$

$$I_{aniso}(\nu_{VH}) = I_{VH}(\nu_{VH})$$

where $I_{VV}(\nu)$ and $I_{VH}(\nu)$ are the experimentally collected Raman intensities of the polarized and depolarized Raman components and ν is the frequency in cm^{-1}. VV means that the polarizer and analyzer are parallel to each other, while VH means that the polarizer and analyzer are perpendicular to each other. Thus, we obtained the isotropic and anisotropic spectrum as shown in table of contents entry in ref. 30. The integrated spectra were collected directly from the Raman spectra without using a polarizer and analyzer in the experimental setup.

With the DFT calculated Gaussian Output File of acetonylacetone, we also get the isotropic and anisotropic spectrum theoretically from the dimer model DFT calculations. Gaussview or Multiwfn can transform the dimer frequencies into Raman spectra. The original output file can be regarded as $I_{VV}(\nu_{VV})$. Since we were interested in the C=O vibration, we focused our attention on the C=O frequency and their depolarization ratio. With the depolarization ratio band corresponding to the Raman activity of C=O vibration, we can get the depolarized Raman activity of C=O vibration. With Gaussview, we can transform the frequencies to the depolarized

Raman spectra, I_{VH} of the C=O vibration. Finally, with $I_{iso}(\nu_{VV}) = I_{VV}(\nu_{VV}) - \frac{4}{3}I_{VH}(\nu_{VH})$, we can get the isotropic Raman activity, I_{iso}spectra (see ESI† for more demonstrations).

III. Results and discussion

We performed full geometry optimization of the monomer and dimer structures of acetonylacetone. In order to establish the most stable conformation as the initial point for further calculations, the molecule was submitted to rigorous conformation analysis with all bonds having free rotation. Fig. 1 shows the optimized monomer and dimer structure of acetonylacetone. No imaginary vibrational frequencies were found in the further calculations. The dimer assembled in a head to tail antiparallel manner through weak intermolecular interactions. All DFT calculated vibrational frequencies, depolarization ratio, and the ZPE corrected total free energy for the acetonylacetone monomer and dimer are given in Table 1. The total free energy of the dimer is lower than the monomer by approximately 3.164 cal mol^{-1}. Thus, the dimer is the thermodynamically favored structure. Table 1 lists a comparison of the B3LYP-D3/6-311++G(d,p) calculated vibrational wavenumber with the experimental FT-Raman and FT-IR values. It is worthy to emphasize that C=O stretching in the monomer has two modes, ν_{11} and ν_{12}; ν_{11} is Raman active but ν_{12} is IR active. These two modes split individually into two pairs of frequencies after the formation of the dimer structure (ν_{11} at 1770 cm^{-1} split into 1768/1760 cm^{-1}, ν_{12} at 1759 cm^{-1} split into 1756/1750 cm^{-1}). The peaks at 1768 cm^{-1} and 1760 cm^{-1} are Raman active, andcan be assigned to the experimental anisotropic Raman frequency at 1718.4 cm^{-1} and isotropic peak at 1710.7 cm^{-1}, respectively (Fig. 3). From the calculations, we can imagine that when the dimer is broken into the monomer, the C=O stretching should blue shift to a higher frequency.

The 36 atoms of the acetonylacetone dimer give rise to 102 normal modes of vibration. The overall 102 normal modes of vibration for this dimer are considered to comprise 96 normal modes arising from the in-phase and out-of-phase coupling of these two acetonylacetone molecules and 6 modes associated with the relative translation and rotation of two acetonylacetone molecules. A detailed description is listed in Table 1. The converted calculated Raman spectra using Multiwfn software are shown in Fig. 2. The corresponding in-phase and out-of-phase vibrational modes may differ in wavenumbers and depolarization ratios and the magnitude of these splitting will depend on the strength of interactions between different parts of the neighboring molecules. The overall agreement between the DFT calculated vibrational wavenumbers and the experimental values is good for acetonylacetone. Fig. 2 displays a comparison of the calculated monomer and dimer Raman spectra with the FT-Raman spectrum and FT-IR spectrum of acetonylacetone. The dashed lines in Fig. 2 indicate the correlation between the vibrational modes of acetonylacetone in the calculated Raman spectra and those corresponding to the fundamental modes of acetonylacetone in the FT-Raman and IR spectrum, respectively. The 1712 cm^{-1} band is assigned to the C=O stretch. The wavenumber difference between the FT-Raman spectrum and FT-IR spectrum is 2.3 cm^{-1}. This wavenumber difference is a key characteristic of the noncoincidence effect; other experimental proofs including the isotropic and anisotropic Raman spectra at different concentrations will be presented later. The largest difference between the calculated monomer and dimer lies in the C=O stretching wavenumber. The wavenumber of the monomer is higher than that of the dimer. Other modes are similar with the calculated monomer and dimer structures. The calculation results show that when acetonylacetone transforms from the dimer to the monomer, the frequency of the C=O stretching increases while other modes remain consistent. From the spectral comparison between the FT-Raman and the calculated monomer and dimer, the spectral pattern of the dimer describes more accurately the liquid acetonylacetone. It needs to be stressed that the listed calculated wavenumbers describe the vibrational frequencies of the molecule in its gaseous phase. Hence, the experimentally observed spectrum of the liquid phase may differ to some extent from the calculated spectrum. In the DFT calculation, the B3LYP function tends to overestimate the wavenumbers of the fundamental modes

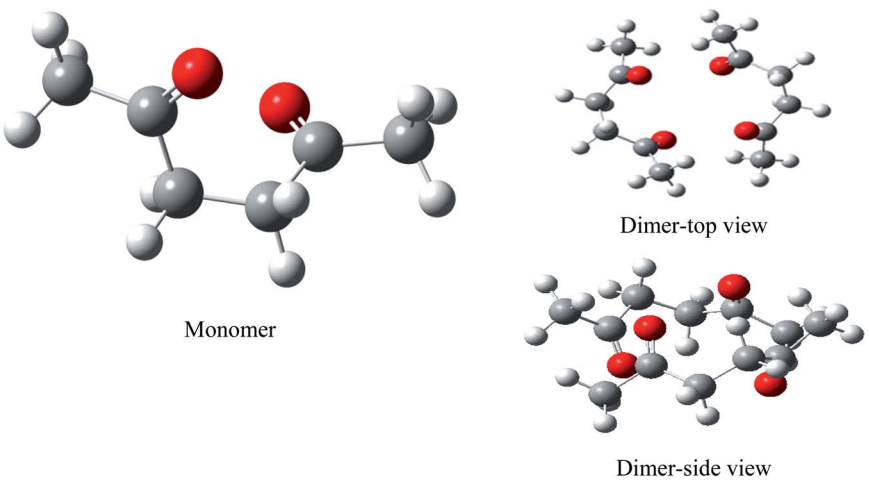

Fig. 1 B3LYP-D3/6-311++G(d,p) computed geometry parameters of acetonylacetone and its aggregates.

Table 1 B3LYP-D3/6-311++G(d,p) computed wavenumbers, depolarization ratios, ZPE corrected total free energies of the acetonylacetone monomer and dimer in the gaseous state

	Computed/cm^{-1}				Experiment/cm^{-1}		
	Monomer freq.		Dimer				
Modes	*cis*	*anti*	Freq.	*D* radio	Raman	IR	Descriptions
ν_1	3144	3138	3141/3138	0.71/0.72			C–H stretch
ν_2	3139	3138	3137/3134	0.68/0.71			C–H stretch
ν_3	3107	3085	3106/3104	0.32/0.72			C–H stretch
ν_4	3094	3085	3097/3095	0.72/0.55			C–H stretch
ν_5	3087	3064	3090/3088	0.75/0.65			C–H stretch
ν_6	3053	3064	3083/3075	0.46/0.74			C–H stretch
ν_7	3033	3034	3044/3038	0.03/0.04			C–H stretch
ν_8	3030	3030	3035/3032	0.25/0.07			C–H stretch
ν_9	3027	3024	3031/3027	0.08/0.07			C–H stretch
ν_{10}	3017	3023	3027/3017	0.03/0.50			C–H stretch
ν_{11}	**1770**	**1781**	**1768/1760**	**0.41/0.32**	**1714S**		**O=C stretch**
ν_{12}	**1759**	**1775**	**1756/1750**	**0.38/0.18**		**1712vs**	**O=C stretch**
ν_{13}	1476	1478	1478/1474	0.45/0.75			H–C–H bend
ν_{14}	1472	1478	1472/1470	0.74/0.65			H–C–H bend
ν_{15}	1467	1468	1466/1465	0.70/0.45			H–C–H bend
ν_{16}	1458	1466	1464/1463	0.74/0.68			H–C–H bend
ν_{17}	1457	1458	1460/1456	0.71/0.74	1455vs	1400w	H–C–H bend + H–C–C–C tors
ν_{18}	1452	1454	1445/1430	0.75/0.74			H–C–H bend
ν_{19}	1390	1401	1401/1394	0.31/0.63			H–C–H bend
ν_{20}	1388	1388	1392/1390	0.69/0.70	1353vw	1365s	H–C–H bend
ν_{21}	1374	1384	1383/1375	0.63/0.72			H–C–H bend
ν_{22}	1355	1333	1373/1370	0.71/0.64			H–C–C bend
ν_{23}	1284	1301	1262/1244	0.60/0.36			H–C–C bend + H–C–C–C tors
ν_{24}	1215	1198	1224/1221	0.70/0.73			H–C–C bend
ν_{25}	1208	1188	1203/1197	0.68/0.63			H–C–C bend
ν_{26}	1175	1172	1183/1182	0.70/0.74			C–C stretch
ν_{27}	1094	1098	1096/1090	0.10/0.05			O=C–C–C out-of-plane bend
ν_{28}	1055	1096	1059/1050	0.29/0.72			C–C stretch
ν_{29}	1021	993	1033/1026	0.75/0.59			H–C–C–C tors
ν_{30}	995	968	984/973	0.33/0.71			C–C stretch + H–C–C–C tors
ν_{31}	966	956	966/958	0.19/0.17			C–C stretch
ν_{32}	891	872	908/894	0.42/0.28			H–C–C bend + H–C–C–C tors + C–C–C–C tors
ν_{33}	835	869	862/862	0.68/0.44			C–C stretch
ν_{34}	768	799	761/752	0.74/0.08	829vs		C–C stretch
ν_{35}	734	729	749/749	0.58/0.02			H–C–C–C tors
ν_{36}	621	602	639/637	0.60/0.73			C–C stretch + O=C–C bend
ν_{37}	556	588	576/574	0.43/0.47			O=C–C bend + C–C–C bend
ν_{38}	530	479	505/485	0.75/0.75			O=C–C bend + H–C–C–C tors + O=C–C–C out-of-plane bend
ν_{39}	467	477	473/455	0.68/0.71			H–C–C–C tors + C–C–C–C tors + O=C–C–C out-of-plane bend
ν_{40}	439	448	452/429	0.74/0.71			C–C–C bend + O=C–C–C out-of-plane bend
ν_{41}	348	316	360/343	0.24/0.34			C–C–C bend
ν_{42}	262	260	271/270	0.27/0.74			C–C–C bend
ν_{43}	234	130	246/232	0.57/0.70			C–C–C bend
ν_{44}	188	109	163/150	0.55/0.66			C–C–C bend
ν_{45}	120	107	139/126	0.70/0.54			H–C–C–C tors
ν_{46}	102	89	114/113	0.71/0.68			H–C–C–C tors + C–C–C–C tors
ν_{47}	56	61	108/97	0.65/0.73			C–C–C–C tors
ν_{48}	45	28	87/81	0.75/0.74			C–C–C–C tors
ν_{49}			72/62	0.69/0.70			Relative rotation
ν_{50}			51/36	0.63/0.75			Relative rotation
ν_{51}			33/26	0.56/0.71			Relative rotation
Sum of electronic and thermal free energies (Kcal mol^{-1})			Momomer	$G = -385.130890$			
			Dimer	$G = -770.264944$	$\Delta G = G(\text{dimer}) - 2G(\text{momomer}) = -0.003164$		
Remarks			In the dimer, there are in-phase and out-of-phase vibrational modes, in-phase vibrational frequency is lower than the out-of-phase vibrational frequency				

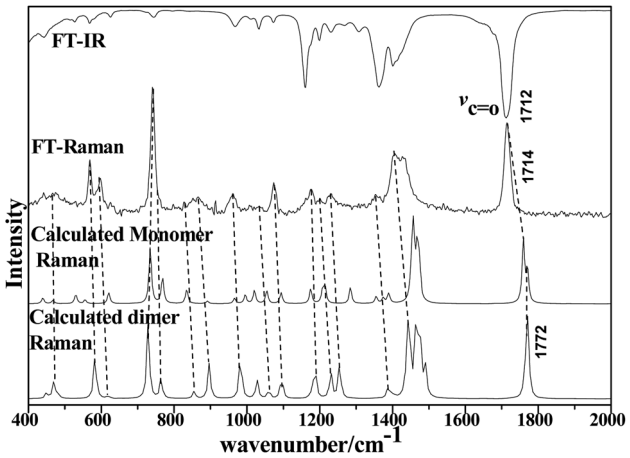

Fig. 2 Comparison of FT-IR and LCM-Raman spectra with calculated Raman and IR spectra of acetonylacetone.

compared to the experimentally observed values due to the combination of electron correlation effects and basis set deficiencies. By comprehensively considering the calculated and experimental FT-Raman spectra, acetonylacetone is prone to present a short dimer order induced by C=O vibrational td–td interactions. While in dilute solution, due to solvation effects and cage effects, where solvent molecules are surrounded by solute molecules that stabilize the solvate, acetonylacetone may present the monomer formation. Thus, the frequency of C=O stretching is influenced by concentration effects.

To characterize the concentration effects, we collected the isotropic and anisotropic spectra of acetonylacetone in a variety of volume fractions, as shown in Fig. 3. They are assigned to the ν_{11}(C=O) stretching mode. The isotropic peak frequencies at 1710.7 cm^{-1} and the anisotropic peak at 1718.4 cm^{-1} were assigned to the calculated wavenumbers at 1760 cm^{-1} and 1768 cm^{-1}, respectively. The corresponding depolarization ratios are 0.32 and 0.41. The dimer model calculations are in good agreement with the experimental non-coincident isotropic and anisotropic Raman data. The isotropic and anisotropic spectra, at a variety of volume fractions of acetonylacetone in CCl_4, are shown in Fig. 3. Fig. 3 demonstrates that both isotropic and anisotropic Raman wavenumbers of the C=O stretch increase with the dilution of acetonylacetone by CCl_4, while the separation between isotropic and anisotropic Raman wavenumbers decrease from 7.66 cm^{-1} in neat acetonylacetone to 1 cm^{-1} at χ_m = 0.05. The FWHM (full width at half maxima) of the C=O stretching modes also gets smaller and the peak gets sharper with decreasing acetonylacetone concentrations. The peak frequencies abstracted from Fig. 3 for isotropic (I_{iso}) and anisotropic (I_{aniso}) C=O stretching Raman spectra are shown in Fig. 4. The Raman peak frequencies of both components show an increase in wavenumber with decreasing solute concentrations. The difference between isotropic (I_{iso}) and anisotropic (I_{aniso}) C=O stretching wavenumbers $\Delta\upsilon_{NCE}$ decreases upon dilution with CCl_4 and reduces to 1.00 cm^{-1} at χ_m = 0.05, as shown in Fig. 5. This experimental data can be explained with our aggregation-induced split theory. Normally, acetonylacetone presents a dimer pattern. The dilution of the solute alters the short-range order of the C=O stretching normal coordinate and the relative alignment of the dimer structure. The solvent molecules diffuse towards the reference molecule and break its structure, thereby weakening the dipole–dipole interactions of solute molecules. Thus, this leads to a decrease in the non-coincidence effect. The breaking of the dimer structure also makes the C=O vibrational wavenumber shift to a higher wavenumber because the calculation shows that the C=O stretching of the monomer lies at a higher wavenumber than that of dimers. This is in accordance with the concentration effect observed in experiments shown in Fig. 3 and 4.

In our study, the NCE of the C=O stretching mode of acetonylacetone is positive, and may be due to the antiparallel C=O side-by-side organization. The antiparallel C=O coupling split the C=O vibrational wavenumber to two. It has been

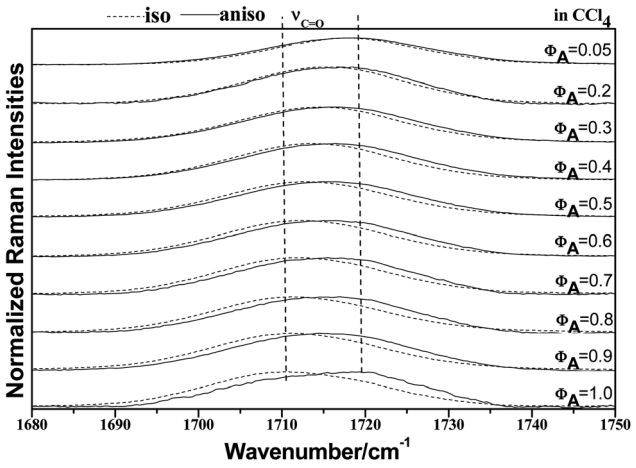

Fig. 3 Isotropic and anisotropic parts of the Raman spectra in the region 1680–1750 cm^{-1} for neat acetonylacetone and nine other volume fractions of acetonylacetone, 0.9, 0.8, 0.70, 0.60, 0.50, 0.40, 0.30, 0.20, and 0.05, in the binary mixture (acetonylacetone + CCl_4).

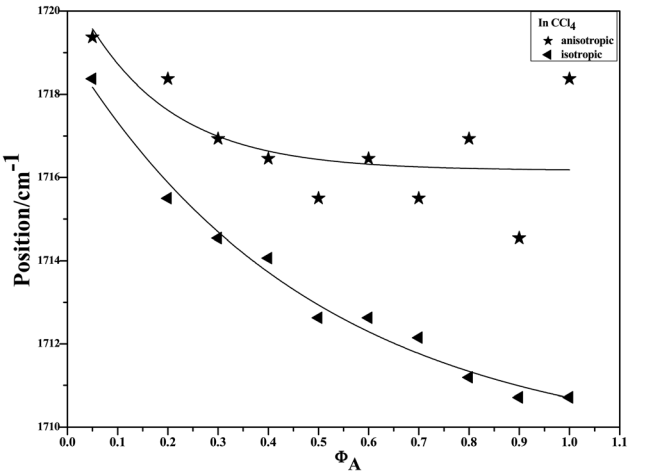

Fig. 4 Variation of isotropic and anisotropic Raman peak frequencies of the C=O stretching mode of acetonylacetone as a function of the solute concentration.

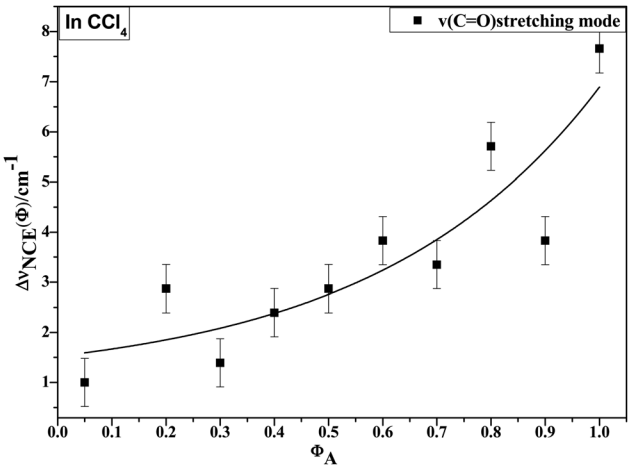

Fig. 5 Variation in NCE of the C=O stretching mode of acetonylacetone as a function of solute volume fraction.

widely known that the NCE represents a spectroscopic manifestation of resonant intermolecular interactions between nearby IR-active oscillators through the transition dipole–transition dipole interaction mechanism.[8–10] The *cis* and *trans* forms of acetonylacetone have C=O Raman activity vibrational frequencies at 1770 cm^{-1} and 1781 cm^{-1}, respectively. We also carried out IRC/path scan for the *cis* to *trans* transformation, as shown in Fig. S1.† This is a barrierless process. In the solution, normally, we believe that acetonylacetone predominantly bears the anti-form but this is not the case for the Raman spectra. Fig. 3 shows a split in the isotropic and anisotropic parts in most of the concentrated solutions. The concentration effect demonstrates that the aggregated structure is formed by intermolecular interactions, instead of intramolecular.

To study the influence of dipole moment of the solvent upon NCE, we collected the isotropic and anisotropic Raman spectra of acetonylacetone in a series of solvents with different static dielectric constant, as shown in Fig. 6. The corresponding NCEs were calculated and are illustrated in Fig. 7. Generally, the value of the NCE declined with an increase in the solvent dielectric constant with the same concentration. This rule is consistent with Logan's theory.[11,35] Especially in water, as shown in Fig. 6, the value of the NCE is nearly equal to zero. From ref. 27 and 28, we speculate that it may be due to the formation of intermolecular hydrogen bonds between protons of water and the carbonyl groups of acetonylacetone, which hinder the dimerization of acetonylacetone molecules, thus making the NCE disappear.

To investigate NCE solvent polarity dependent properties and demonstrate the rationality of the dimer model, the polarizable continuum model (PCM) was applied to calculate the dimer structure at the hybrid B3LYP-D3 levels of theory with the 6-311++G(d,p) basis set using the Gaussian 09 program. The solvent polarity influence, the optimized geometry, and the corresponding vibrational frequencies were obtained. Table S1† shows the DFT/PCM calculated C=O vibrational frequencies, depolarization ratios, dielectric constants (ε), dipole moments (μ)/D, and $\Delta\nu_{NCE}$ in a variety of solvents. With a decrease in the solvent dielectric constant, the two monomers of the acetonylacetone dimer became closer and the value of the NCE increased. These results are consistent with the experimental results shown in Fig. 7. Simultaneously, this verifies that a strong polar solvent will weaken the dimer structure of acetonylacetone in the mixture while a nonpolar solvent can reinforce the dimer structure. All results that are obtained from experiments, the theoretical dimer model, and DFT calculations demonstrate a consistent picture of the relationship between the NCE behavior, a spectroscopic feature of vibrational Raman bands, and the effect of dipolar interactions in liquid mixtures at molecular level.

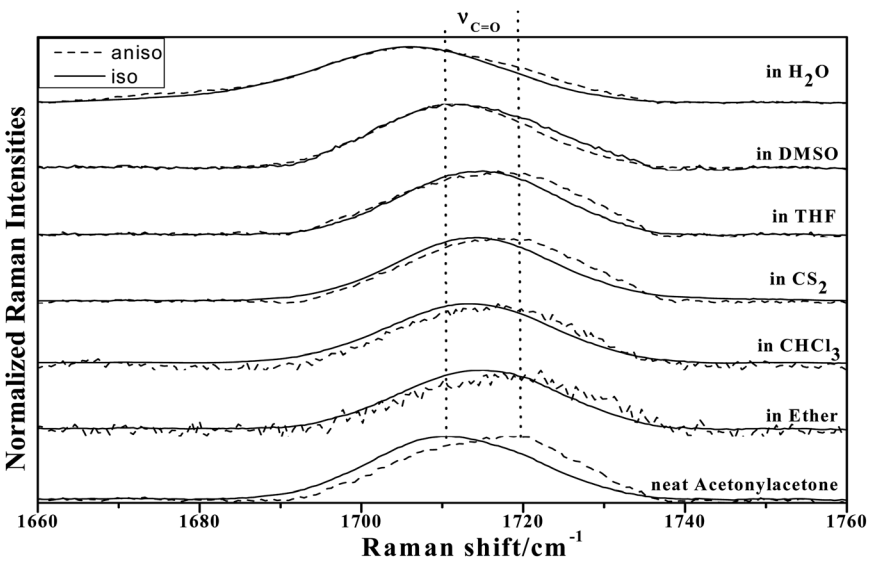

Fig. 6 The isotropic and anisotropic parts of ν_{12}(C=O) vibrational Raman spectra of acetonylacetone in the binary mixture with different solvents ($\varphi_A = 0.500$).

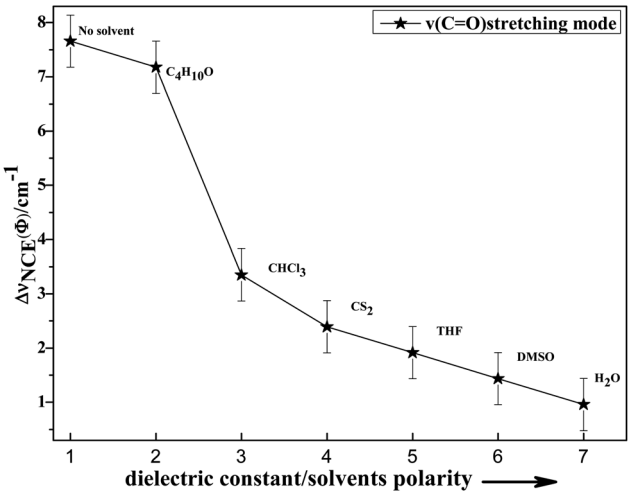

Fig. 7 Variation in NCE of the C=O stretching mode of acetonylacetone as a function of the solvent dielectric constant.

IV. Conclusion

The Raman spectroscopic noncoincidence effect of the ν(C=O) band of acetonylacetone in a binary mixture has been reported and $\Delta\upsilon_{nce}$ has been measured for different concentrations. The monomer (*cis* and *trans* forms) and dimer of acetonylacetone were calculated at the B3LYP-D3/6-311++G (d,p) level of theory, which makes it easy to accurately investigate the molecular interactions through observation of concentration dependent and NCE properties. During the dilution process, the solute–solvent interactions weaken the dipole–dipole interactions, which results in the Raman spectra gradually transforming from dimer to monomer character, indicated by a blueshift in the C=O stretching. Density functional theory (DFT) calculations based on the aggregation model provide satisfactory results and fit well with the experimental findings while the *cis* and *trans* forms cannot explain the Raman behavior; on the other hand, this model and experimental data verified the rationality of the aggregation-induced split theory. Solvent dependent experiments show that the value of NCE decreased with an increase in the dielectric constant of the solvent, for the same concentration.

Author's contributions

All authors contributed equally to this work.

Data availablity

The data that supports the findings of this study are available within the article and its ESI.†

Conflicts of interest

There are no conflicts of interest to declare.

Acknowledgements

This work was supported by grants from the National Natural Science Foundation of China (No. 21873084 and 21473161), Zhejiang Provincial Natural Science Foundation of China (LZ17B030001), Alexander von Humboldt Foundation (No. 1141172), and Zhejiang SCI-TECH University for 521 distinguished scholar's scheme.

References

1 J. H. Baraban, P. B. Changala, G. C. Mellau, J. F. Stanton, A. J. Merer and R. W. Field, Spectroscopic characterization of isomerization transition states, *Science*, 2015, **350**(6266), 1338–1342.
2 J.-X. Cheng and X. S. Xie, Vibrational spectroscopic imaging of living systems: An emerging platform for biology and medicine, *Science*, 2015, **350**(6264), aaa8870.
3 V. H. Paschoal, L. F. O. Faria and M. C. C. Ribeiro, Vibrational Spectroscopy of Ionic Liquids, *Chem. Rev.*, 2017, **117**(10), 7053–7112.
4 F. Billes, I. Mohammed-Ziegler and H. Mikosch, Methanol in its own gravy. A PCM study for simulation of vibrational spectra, *Phys. Chem. Chem. Phys.*, 2011, **13**(17), 7760–7772.
5 W.-H. Su and D.-W. Sun, Fourier Transform Infrared and Raman and Hyperspectral Imaging Techniques for Quality Determinations of Powdery Foods: A Review, *Compr. Rev. Food Sci. Food Saf.*, 2018, **17**(1), 104–122.
6 J.-B. Wu, M.-L. Lin, X. Cong, H.-N. Liu and P.-H. Tan, Raman spectroscopy of graphene-based materials and its applications in related devices, *Chem. Soc. Rev.*, 2018, **47**(5), 1822–1873.
7 Y. Cai, Z. Wei, C. Song, C. Tang, W. Han and X. Dong, Optical nano-agents in the second near-infrared window for biomedical applications, *Chem. Soc. Rev.*, 2019, **48**(1), 22–37.
8 H. Y. Juan, W. C. Lin, Y. L. Wu and J. H. Perng, Substituent effects in porphyrin dimer complexes studied by IR spectroscopy, *Polyhedron*, 2008, **27**(16), 3377–3382.
9 S. Shigeto, C. F. Chang and H. Hiramatsu, Directly Probing Intermolecular Structural Change of a Core Fragment of beta(2)-Microglobulin Amyloid Fibrils with Low-Frequency Raman Spectroscopy, *J. Phys. Chem. B*, 2017, **121**(3), 490–496.
10 G. Fini, P. Mirone and B. Fortunat, Evidence for Short-Range Orientation Effects in Dipolar Aprotic Liquids from Vibrational Spectroscopy 1. Ethylene and Propylene Carbonates, *J. Chem. Soc., Faraday Trans.*, 1973, **69**(8), 1243–1248.
11 D. E. Logan, THE RAMAN NONCOINCIDENCE EFFECT IN DIPOLAR BINARY-MIXTURES, *Chem. Phys.*, 1989, **131**(2–3), 199–207.
12 M. G. Giorgini, Raman noncoincidence effect: A spectroscopic manifestation of the intermolecular vibrational coupling in dipolar molecular liquids, *Pure Appl. Chem.*, 2004, **76**(1), 157–169.
13 M. G. Giorgini, M. Musso and H. Torii, Concentration-dependent frequency shifts and Raman spectroscopic noncoincidence effect of the C=O stretching mode in

dipolar mixtures of acetone/dimethyl sulfoxide. Experimental, theoretical, and simulation results, *J. Phys. Chem. A*, 2005, **109**(26), 5846–5854.

14 H. Torii, Effects of intermolecular vibrational coupling and liquid dynamics on the polarized Raman and two-dimensional infrared spectral profiles of liquid N,N-dimethylformamide analyzed with a time-domain computational method, *J. Phys. Chem. A*, 2006, **110**(14), 4822–4832.

15 M. G. Giorgini, H. Torii, M. Musso and G. Venditti, Influence of ions on the structural organization of dipolar liquids probed by the noncoincidence effect: Experimental and quantum chemical results, *J. Phys. Chem. B*, 2008, **112**(25), 7506–7514.

16 H. Torii, Y. Osada and M. Iwami, Merged and separate band profiles arising from resonantly coupled vibrational modes of liquid mixtures: theoretical study, *J. Raman Spectrosc.*, 2008, **39**(11), 1592–1599.

17 M. G. Giorgini, H. Torii and M. Musso, The influence of alkaline earth ions on the structural organization of acetone probed by the noncoincidence effect of the nu(C=O) band: experimental and quantum chemical results, *Phys. Chem. Chem. Phys.*, 2010, **12**(1), 183–192.

18 H. Torii, Intermolecular Electron Density Modulations in Water and Their Effects on the Far-Infrared Spectral Profiles at 6 THz, *J. Phys. Chem. B*, 2011, **115**(20), 6636–6643.

19 G. Upadhyay, T. G. Devi, R. K. Singh, A. Singh and P. R. Alapati, Solvent dependent frequency shift and Raman noncoincidence effect of S=O stretching mode of Dimethyl sulfoxide in liquid binary mixtures, *Spectrochim. Acta, Part A*, 2013, **109**, 239–246.

20 H. Torii, Amide I Vibrational Properties Affected by Hydrogen Bonding Out-of-Plane of the Peptide Group, *J. Phys. Chem. Lett.*, 2015, **6**(4), 727–733.

21 F. Wu, H. Wang and X. Zheng, Concentration-dependent frequency shifts of the CS stretching modes in ethylene trithiocarbonate studied by Raman spectroscopy, *J. Raman Spectrosc.*, 2015, **46**(6), 591–596.

22 R. Zhou, F. Wu, X. Zhou, H. Wang and X. Zheng, The structural configurations of Ethylene Trithiocarbonate in the binary mixture (SCS2CH2CH2+CFICl3) investigated by polarized Raman: Experimental and quantum chemical results, *J. Mol. Struct.*, 2017, **1129**, 205–210.

23 Y. Gong, M. Zhou and L. Andrews, Spectroscopic and Theoretical Studies of Transition Metal Oxides and Dioxygen Complexes, *Chem. Rev.*, 2009, **109**(12), 6765–6808.

24 Q. Wang, S. Pan, S. Lei, J. Jin, G. Deng, G. Wang, L. Zhao, M. Zhou and G. Frenking, Octa-coordinated alkaline earth metal-dinitrogen complexes M(N-2)(8) (M=Ca, Sr, Ba), *Nat. Commun.*, 2019, **10**, 3375.

25 M. Liu, Y. Zhao, F. Wu, H. Wang and X. Zheng, Argon matrix Raman spectroscopic and aggregation model density function theoretical study of methyl isothiocyanate, *J. Raman Spectrosc.*, 2019, **50**(8), 1217–1225.

26 W. W. Xu, F. Q. Wu, Y. Y. Zhao, R. Zhou, H. G. Wang, X. M. Zheng and B. K. Ni, Study on the noncoincidence effect phenomenon using matrix isolated Raman spectra and the proposed structural organization model of acetone in condense phase, *Sci. Rep.*, 2017, **7**, 43835.

27 R. Srinivasan, J. S. Feenstra, S. T. Park, S. Xu and A. H. Zewail, Direct determination of hydrogen-bonded structures in resonant and tautomeric reactions using ultrafast electron diffraction, *J. Am. Chem. Soc.*, 2004, **126**(8), 2266–2267.

28 J. Emsley and N. J. Freeman, β-diketone interactions: Part 5. Solvent effects on the keto = enol equilibrium, *J. Mol. Struct.*, 1987, **161**(c), 193–204.

29 W. Xu, Y. Sun, X. Dong, S. Li, H. Wang, J. Xue and X. Zheng, Local order and vibrational coupling of the C=O Stretching Mode of gamma-Caprolactone in liquid binary mixtures, *Sci. Rep.*, 2017, **7**, 12182.

30 W. Xu, H. Wang, Y. Tao and X. Zheng, The structural organization of N-methyl-2-pyrrolidinone in binary mixtures probed by Raman spectroscopy: Experimental and quantum chemical results, *J. Raman Spectrosc.*, 2018, **49**(2), 362–371.

31 H. Ouyang, M. Liu, Y. Zhao, H. Wang and X. Zheng, Noncoincidence Effects of Dimethyl Carbonate in Binary Mixtures Probed by Raman Spectroscopy: Experimental and DFT Calculations, *ACS Omega*, 2019, **4**(6), 11074–11081.

32 M. J. Frisch, G. W. Trucks, H. B. Schlegel, G. E. Scuseria, M. A. Robb, J. R. Cheeseman, J. A. Montgomery Jr, T. Vreven, K. N. Kudin, J. C. Burant, J. M. Millam, S. S. Iyengar, J. Tomasi, V. Barone, B. Mennucci, M. Cossi, G. Scalmani, N. Rega, G. A. Petersson, H. Nakatsuji, M. Hada, M. Ehara, K. Toyota, R. Fukuda, J. Hasegawa, M. Ishida, T. Nakajima, Y. Honda, O. Kitao, H. Nakai, M. Klene, X. Li, J. E. Knox, H. P. Hratchian, J. B. Cross, C. Adamo, J. Jaramillo, R. Gomperts, R. E. Stratmann, O. Yazyev, A. J. Austin, R. Cammi, C. Pomelli, J. W. Ochterski, P. Y. Ayala, K. Morokuma, G. A. Voth, P. Salvador, J. J. Dannenberg, V. G. Zakrzewski, S. Dapprich, A. D. Daniels, M. C. Strain, O. Farkas, D. K. Malick, A. D. Rabuck, K. Raghavachari, J. B. Foresman, J. V. Ortiz, Q. Cui, A. G. Baboul, S. Clifford, J. Cioslowski, B. B. Stefanov, G. Lui, A. Liashenko, P. Piskorz, I. Komaromi, R. L. Martin, D. J. Fox, T. Keith, M. A. Al-Laham, C. Y. Peng, A. Nanayakkara, M. Challacombe, P. M. W. Gill, B. Johnson, W. Chen, M. W. Wong, C. Gonzalez and J. A. Pople, *Gaussian 03(1), Revision C.02, Gaussian 03, Revision B.02*, Gaussian, Inc., Pittsburgh, PA, 2003.

33 T. Lu and F. Chen, Multiwfn: a multifunctional wavefunction analyzer, *J. Comput. Chem.*, 2012, **33**(5), 580–592.

34 G. Keresztury, S. Holly, G. Besenyei, J. Varga, A. Wang and J. Durig, Vibrational spectra of monothiocarbamates-II. IR and Raman spectra, vibrational assignment, conformational analysis and ab initio calculations of S-methyl-N, N-dimethylthiocarbamate, *Spectrochim. Acta, Part A*, 1993, **49**(13–14), 20072019–20172026.

35 D. E. Logan, The Non-Coincidence Effect in the Raman-Spectra of Polar Liquids, *Chem. Phys.*, 1986, **103**(2–3), 215–225.